Available online at www.sciencedirect.com
SCIENCE DIRECT®
Journal of Nuclear Materials 350 (2006) 135–146
journal of nuclear materials
www.elsevier.com/locate/jnucmat

Influence of metallurgical variables on delayed hydride cracking in Zr–Nb pressure tubes

P. Cirimello, G. Domizzi *, R. Haddad

Unidad de Actividad Materiales, Centro Atómico Constituyentes, Comisión Nacional de Energía Atómica, Av. Gral. Paz 1499, (B1650KNA) San Martín, Buenos Aires, Argentina

Received 26 July 2005; accepted 1 December 2005

Abstract

During service, Zr–2.5Nb pressure tubes of nuclear power reactors may be prone to suffer from crack growth by delayed hydride cracking (DHC). For a given hydrogen plus deuterium concentration there is a critical temperature (T_C) below which DHC may occur. In this work, T_C was measured for specimens cut from pressure tubes made in Canada (CANDU) and in Russia (RBMK). Hydrogen was added to the specimens to get concentrations ranging from 24 to 60 wt ppm. It was found that T_C was higher than the corresponding precipitation temperature. The crack propagation velocity (V_P), measured in axial direction, increases from a minimum at T_C to a maximum at a temperature close but higher than the precipitation temperature. At lower temperatures, when hydride precipitates are present in the bulk, V_P follows an Arrhenius law: $V_P = A\exp(-Q/RT)$, with an activation energy Q of 66–68 kJ/mol for both tubes. The RBMK material presented lower velocities than CANDU one.

PACS: 81.40

1. Introduction

In CANDU nuclear reactors, fuel bundles are located in Zr–2.5Nb pressure tubes (PT). At operation, PT's gradually pick up deuterium which adds up to the initial hydrogen concentration. Depending on the operation conditions (temperature, thermal cycle and hydrogen–deuterium concentration attained), Zr alloys may become susceptible to the crack process known as delayed hydride cracking (DHC). This type of failure is produced by preferential and repeated precipitation of hydrides at stress raisers and their subsequent fracture, causing crack growing in steps [1]. A quantitative model which describes the crack propagation process has been developed by Dutton et al. [2]. This model predicts that the temperature dependence of the crack velocity resides largely in the product of the hydrogen diffusion coefficient and the terminal solubility for dissolution of hydrogen.

The hysteresis between precipitation and dissolution solvi is well known: the terminal solid solubility for precipitation (TSSP) is higher than TSSD (dissolution) [3]. This hysteresis is produced by the plastic

* Corresponding author. Tel.: +54 11 6772 7287; fax: +54 11 6772 7362.
E-mail address: domizzi@cnea.gov.ar (G. Domizzi).

0022-3115/$ - see front matter © 2006 Elsevier B.V. All rights reserved.
doi:10.1016/j.jnucmat.2005.12.002

deformation introduced in both matrix and hydride during hydride precipitation. On cooling samples from different T_S temperatures, Pan et al. [4] measured two different curves for precipitation. When the sample was treated at $T_S = 420$–450 °C:

$$\mathrm{TSSP1} = 2.47 \times 10^4 \exp(-25\,840/RT) \quad (1)$$

and when $T_S = 220$–368 °C:

$$\mathrm{TSSP2} = 3.15 \times 10^4 \exp(-27\,990/RT), \quad (2)$$

where $R = 8.31$ J/K mol and T is the absolute temperature.

Early studies on DHC supported the idea that the presence of hydride particles in the bulk was a necessary condition for DHC to occur [2,5]. Based on these ideas, Puls [6] included the concept of hysteresis in the mentioned DHC model. He assumed that the hydride precipitation near the stress raiser obeys TSSP curve but, in the bulk the hydrogen concentration is in equilibrium with the dissolving hydride particles (TSSD) when the test temperature is approached from below, and with TSSP when approached from above [7].

More recently, Shi et al. [8] measured a critical temperature T_C, at which DHC would initiate when approaching to test temperature (T_T) by cooling from above the temperature corresponding to the TSSD solvus (T_D). For different hydrogen concentrations T_C takes values between T_P (precipitation temperature determined by TSSP) and T_D. So, hydride precipitation may occur at the crack tip, even if no hydride is present in the bulk.

As pointed by Shi et al. [8], the high stress gradient at the crack tip lowers the chemical potential of hydrogen in the surroundings and produces the driving force for hydrogen diffusion to the crack tip. When the temperature is cooled down to T_C, the hydrogen concentration at the crack tip equals the TSSP, resulting in hydride precipitation and crack propagation.

Therefore, while considering T_P as the limit temperature for starting DHC would be dangerous, considering T_D might be too conservative. In this work the highest temperature (T_C) for DHC initiation during cooling was measured for two pressure tube materials. Knowledge of this value as a function of hydrogen content may be relevant to evaluate the risk of failure by DHC during hot shutdown of a nuclear power reactor.

Shi et al. [8] used two different methods (A and B) to measure T_C. In procedure A, the specimen was heated, without load, 50 °C above T_D, then cooled down to a test temperature (T_T) 20 °C above T_D, then loaded. If no cracking was detected in 24 h or more, the temperature was reduced in small steps until DHC started. After cracking was established, the specimen was unloaded and the whole cycle repeated. Procedure B was similar but, in the first cycle T_T was a temperature at which cracking was expected, and in subsequent cycles the temperature was increased in steps until cracking was not observed after waiting more than 96 h. They found that T_C tends to increase with the number of cycles. The authors [8] proposed two different explanations for this effect. The DHC process in the first cycle was initiated from a fatigue crack, whereas in the subsequent cycles the initial crack was produced by the previous DHC cycle. For this reason, they assumed that a higher level of hydrostatic stress at the tip of a DHC crack may be expected; this requires a lower quantity of hydrides for cracking to initiate, therefore DHC would start at a higher T_C. Another difference between fatigue and DHC cracks, taken into account by the authors, was the memory effect; the nucleation of hydrides at the tip of a DHC crack is favored by the matrix deformation introduced by the precipitation during the prior thermal cycle; consequently, T_C would be higher. In this paper an attempt is made to elucidate this point.

In nuclear reactors, the leak-before-break (LBB) criterion requires the crack be detected by the leak detection system, so the reactor can be shut down before the crack reaches the critical length. The available time, before catastrophic rupture occurs, depends on the initial crack size at wall penetration and shape, the critical crack length and the velocity of crack propagation (V_P). Hence, it is very important to know V_P in the axial direction.

When DHC tests were carried out by cooling the specimens from above T_D to a temperature T_T, lower than the precipitation temperature T_P, the measured crack growth rate vs T_T follows an Arrhenius relationship [5,9]. No V_P data are reported for T_T higher than T_P. In the present paper the crack propagation was measured, for different hydrogen concentrations and temperatures lower than T_C, on specimens machined from a Canadian and a Russian PT's.

2. Experimental method

2.1. Test specimens

In the frame of an IAEA's Coordinated Research Program (CRP) [10], material from two Zr–2.5Nb

PT's was analyzed. One PT (CANDU) was produced in Canada and the other one (RBMK TMT 1) was made in Russia.

At the last stage of fabrication route, CANDU PT's received an autoclave treatment at 400 °C during 24 h, while the TMT 1 Russian PT's were aged 24 h at 515 °C. Table 1 shows the yield stress data, measured along transverse direction of PT [10].

The as-received materials were characterized by optical and electron microscopy. Vickers microhardness was measured on radial–circumferential (RC) and radial–axial (RA) planes, with a 200 g load.

Sections of 77 mm by 35 or 70 mm by the thickness of the PT were electrolytically hydrided in 0.1 M H_2SO_4 solution at 60 °C, during the time required to obtain a hydride layer thick enough to exceed the required hydrogen concentration. After that, each section received two heat treatments in order to produce a uniform hydride distribution. The temperature values of the first heat treatment were chosen to attain different hydrogen concentrations approximately in the range between 30 and 70 ppm. The homogenization temperature was calculated according to Kearns' TSS curve [11], as it was recommended in the IAEA guidelines [12]. The heat treatment duration was determined as $t = (x/2)^2/D$, where x is the sample thickness and D the diffusion coefficient [13]. In order to avoid the re-absorption of hydrogen by the hydride surface layer during cooling, the samples were fast cooled in air. After that, the remaining layer was removed by grinding. All samples received a second thermal treatment at 350 °C during 2.5 h. Then, they were furnace cooled in order to increase the hydride length and obtain a hydride distribution similar to that produced under reactor service conditions.

Curved compact toughness specimens (CCT), analogous to ASTM E-399 standard [14] were machined from the hydrided sections (Fig. 1). The specimens were fatigue pre-cracked with the crack on the radial–axial (RA) plane and the crack propagation direction along the axial direction of the PT.

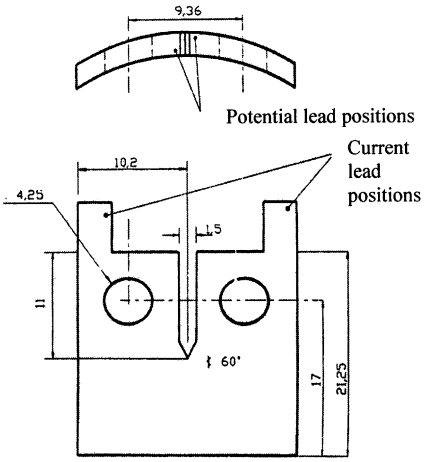

Fig. 1. Scheme of the CCT specimens, dimensions in mm.

All the specimens have been labeled using the following code: the letters C and R correspond to CANDU and RBMK, respectively, the first number corresponds to the section from which the specimen was extracted and the last number is the ID mark.

A small bit was withdrawn from each section and analyzed by hot vacuum extraction mass spectrometry (HVEMS) to measure its hydrogen content, measurements were made in Chalk River Laboratories, Chalk River, Ont., Canada.

Table 1
Yield stress values

Material	Test temperature (°C)	0.2% Yield stress (MPa)
CANDU	20	803
	250	567
RBMK	20	659
	250	494
	300	484

Test direction: transverse [10].

2.2. DHC tests

Tests were made in a dead-weight lever arm testing machine; cracking was monitored by the direct current potential drop method (DCPD) [15]. This method essentially consists in monitoring a signal proportional to the electric resistance of the specimen that rises as the crack propagates. For each specimen, a first test allowed to determine T_C and a second test the velocity V_P.

2.2.1. T_C determination tests

The procedure used to determine the critical temperature (T_C) was similar to the procedure A employed by Shi et al. [8] with some differences: the specimens were heated without load to $T_S = 330$ °C (which is, in all cases, a temperature higher than T_D). The heating rate was between 3 and 5 °C/min. After a soaking time of 1 h the specimens were cooled down at 1–2 °C/min to a test

temperature T_T lower than T_D but higher than T_P. No undercooling by values higher than 1 °C was permitted on reaching T_T. After 0.5 h at T_T, the specimens were loaded to a stress intensity factor, K_I, of about 15 MPa $m^{1/2}$. If no cracking was detected after 2 h, the temperature was reduced in successive ΔT steps until cracking was detected. Then the specimen was unloaded. This cycle was performed twice using values of $\Delta T = 4$ °C in the first cycle and 2 °C in the next one; this way, a quite accurate determination was accomplished in a limited period of time.

In some specimens, a third cycle with $T_S =$ 430 °C was made. The objective of this cycle was to analyze the memory effect at the crack tip.

2.3. V_P measurement tests

In order to use one single specimen to measure the crack growth rate at different T_T's, it is necessary to differentiate each propagation stage on the fracture surface. With this purpose, two different procedures were applied: (a) overloading method and (b) oxidation method.

(a) *Overloading method:* The specimen was heated up to 330 °C, held at this temperature for 1 h and cooled to T_T. After 0.5 h it was loaded and held at temperature during enough time to produce a measurable crack growth (typically 2 h). When this time elapsed, an overload was applied to mark the fracture surface. After 2 min the overload was removed and the temperature was decreased to a new T_T value and the process repeated.

(b) *Oxidation method:* The specimen was heated up to 330 °C, held at this temperature for 1 h and cooled to T_T. After 0.5 h it was loaded and held at T_T during 2 h. Then, the specimen was unloaded and the temperature was raised to a new T_S value higher than T_D but lower than 330 °C. It was held 1 h at this temperature to produce a staining oxide layer on the fracture surface. Then, the specimen was cooled to a new T_T value. This process was repeated in each propagation stage, to make them distinguishable through the different colors which correspond to the diverse oxidation levels.

Whereas the overloading method worked well in tests performed with the CANDU material, it brought experimental problems when dealing with RBMK specimens: crack arresting, inconsistent changes in slopes, etc. So the oxide method was adopted in these cases.

After the DHC test was finished, the specimens were broken open by fatigue. Then, the average crack propagation (da) was measured using the nine lines method recommended by the ASTM E813-81 [16] for each stage of the test. The propagation time (dt) was obtained from the DCPD record. The crack growth rate was calculated as $V_P = da/dt$.

3. Results and discussion

3.1. Material characterization

Figs. 2 and 3 show the microstructure of CANDU and RBMK materials, respectively. Two phases are present in both tubes: α (dark) and β (clear). The CANDU material presents the microstructure usually found in this kind of PT, α grains

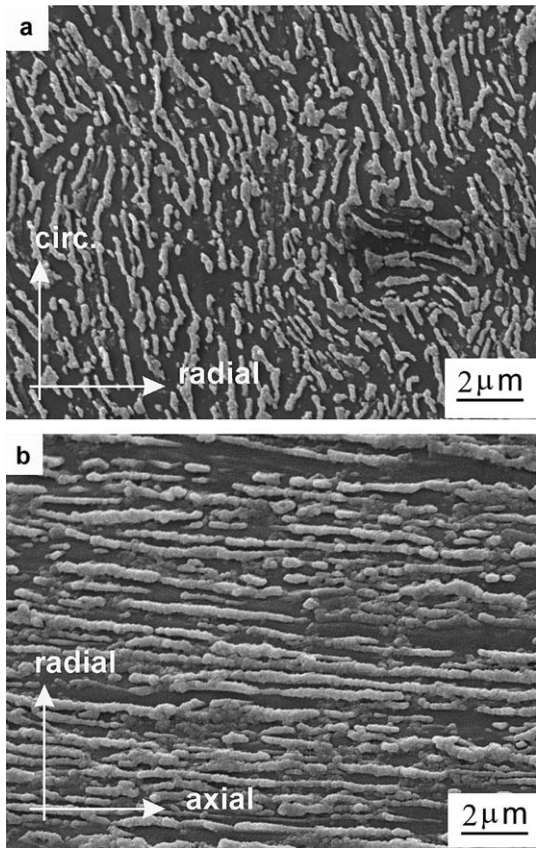

Fig. 2. Microstructure of CANDU pressure tube: (a) radial–circumferential plane and (b) radial–axial plane.

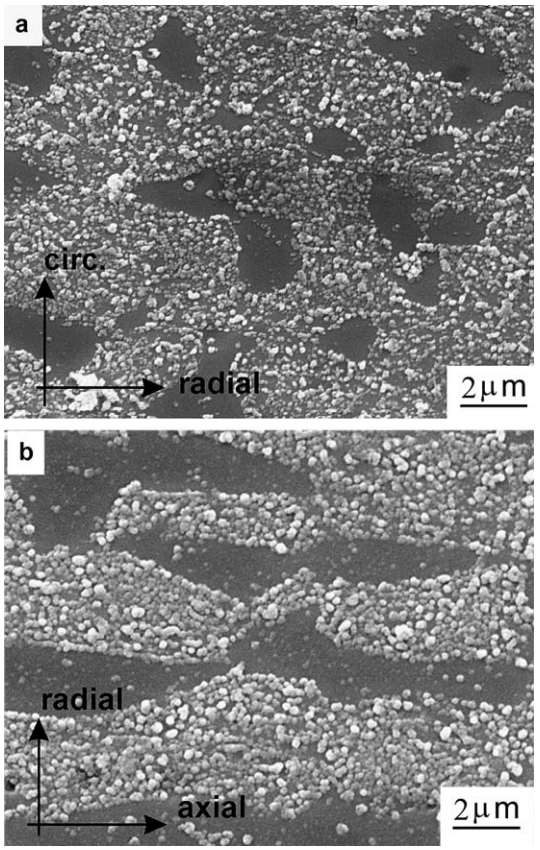

Fig. 3. Microstructure of RBMK pressure tube: (a) radial–circumferential plane and (b) radial–axial plane.

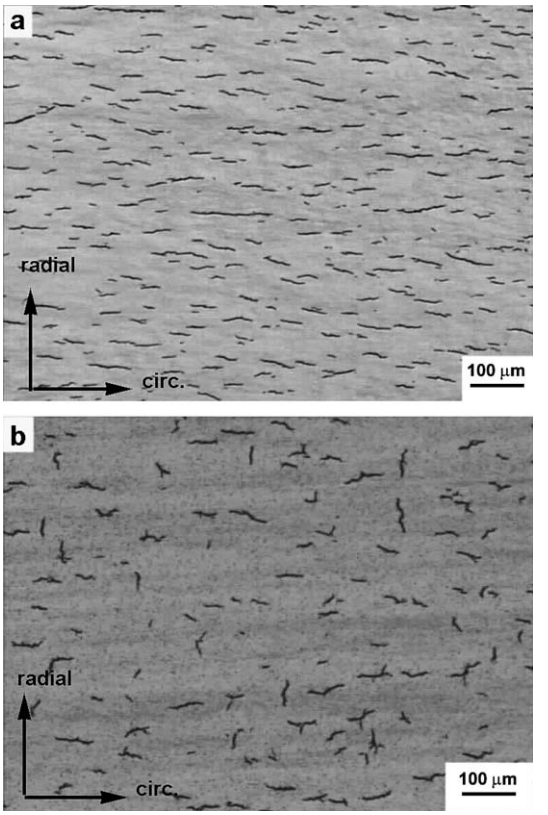

Fig. 4. Hydride distribution on radial–circumferential plane in (a) CANDU specimen with 60 ppm and (b) RBMK specimen with 30 ppm.

elongated in the axial direction and β-phase platelets distributed around α grains. In RBMK material, instead, the α grains are equiaxed and β phase is spheroidized. Micro-hardness values are shown in Table 2. Consistently with the observed microstructure, the Russian PT presents lower hardness and more isotropic behavior than the Canadian one.

After hydriding, both materials present hydride precipitates like thin platelets less than 1 μm thick. In CANDU PT the platelets lie, preferentially, on the axial–circumferential plane even in the specimens with highest hydrogen concentration (Fig. 4(a)). In RBMK, instead, there is a greater number of platelets oriented on the radial–axial plane (Fig. 4(b)).

Table 3 reports the temperature of the first heat treatment. The values measured by HVEMS are reported in the third column while fourth and fifth columns show the concentration calculated by the TSS curve measured by Kearns [11] and Jovanovic [17], respectively. Fig. 5 shows the concentration values measured for CANDU samples, RBMK and TSS best fit curves obtained by different authors [3,4,9,17–19]. The comparison of these results shows that the hydrogen concentrations calculated according [11] are higher than those measured. In two cases (specimens C-1-1 and C-4-2) these discrepancies may be originated in some uncertainty in the temperature measurement; however, in all the other cases this parameter was properly controlled. It is also possible, instead, that the TSS curve of Kearns is not the most appropriate one for Zr–Nb alloys.

Table 2
Micro-hardness, 200 g

Material	Section	Vickers hardness
CANDU	RC	272.7
	RA	341.0
RBMK	RC	238.3
	RA	249.9

Table 3
Temperature of the first heat treatment performed on tested materials

Specimen	First HT (°C)	Hydrogen concentration (ppm)		
		Measured C_0	Kearns [11]	Jovanovic [17]
C-1-1	256	24	35.2	31.1
C-2-1	265	34	40.3	35.4
C-3-3	294	53	60.7	51.7
C-4-2	306	60	71.1	59.9
R-1-1	254	30	34.1	30.3
R-2-2	292	47	59.1	50.5
R-3-2	307	56	72.0	60.6

Hydrogen concentration: measured values for CANDU and RBMK pressure tubes and calculated from Kearns for Zr [11] and from Jovanovic for Zr–2.5%Nb [17].

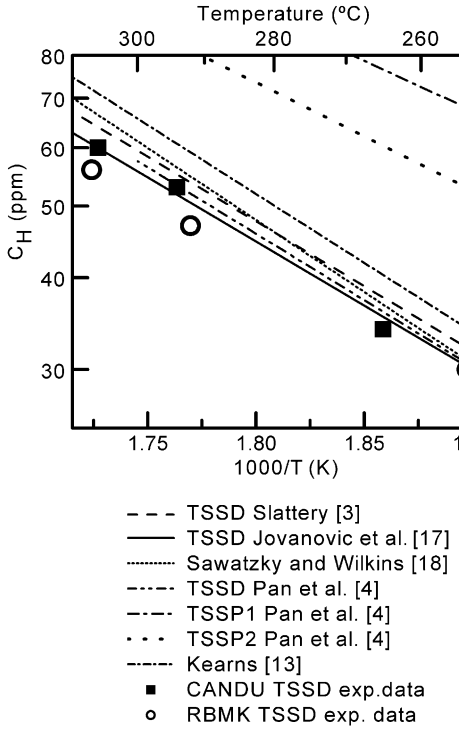

Fig. 5. Measured values of terminal solid solubility and fit curves from different authors (3,4,17,18 were calculated from Zr–2.5Nb data and 13 is and average from Zr, Zry-2 and Zry-4 data).

There is a much better agreement between the experimental values of this work and the TSSD measured in Zr–2.5Nb by Pan et al. [4], Jovanovic et al. [17], Sawatzky and Wilkins [18] and Slattery [3]. The TSSD curve from Jovanovic [17] was measured in Zr–2.5%Nb PT alloy using a method similar to the first heat treatment employed in this work (diffusion anneal of a sample with a previous hydride layer). TSSP curves are also plotted for comparison.

3.2. T_C determination

Table 4 reports the T_C values obtained in CANDU specimens, which were tested in successive cycles. The first cycle (cycle 1) differed from the others in that the initial crack was produced by fatigue and consequently there was no hydride at the crack tip. In the other cycles, when the specimen was heated up to $T_S = 330$ °C, hydrides previously formed at the crack tip were dissolved, but the plastic deformation produced during precipitation should have remained. Under this condition, precipitation at DHC test temperature should have been favored by the memory effect. On the contrary, when $T_S = 430$ °C, any plastic deformation must have been eliminated [3]. In the cycles where $T_S = 430$ °C, TSSP at the crack tip should coincide with TSSP1, while TSSP2 should be the concentration when $T_S = 330$ °C. As TSSP1 is higher than TSSP2, a lower value of T_C should be measured in the cycles having $T_S = 430$ °C. This result was not obtained at all in this work, as can be seen in Table 4. No difference was detected in T_C when the specimen was previously heated up to 330 °C or 430 °C.

Table 4
T_C values measures with different T_S

Specimen	C_H (wt ppm)	Cycle	T_S (°C)	T_C (°C)
C-4-2	60	1	330	283
		2	330	283
		3	430	285
C-4-3		3	330	293
		5	330	293
		7	430	293
C-3-2	53	2–5	330	273–275
		6	430	275

The non-reported cycles presented measurement troubles.

A possible explanation is that the hydrides at the crack tip were quite fractured and no plastic deformation remained around it.

All other specimens were tested with $T_S = 330$ °C and the T_C values obtained in the first cycle (fatigue initial crack) and second cycle (DHC initial crack) were similar. Hence, it is possible to assure that, under the present test conditions, the type of initial crack does not affect the critical temperature for DHC propagation.

T_C values measured in CANDU and RBMK specimens are reported in Tables 5 and 6, respectively. Temperatures for precipitation (T_P), calculated with Eq. (2) (TSSP2), are also reported for comparison. The measured values of T_C are always higher than T_P, these results corroborate that DHC is possible even if no hydrides are precipitated in the material bulk. Fig. 6 shows on a $\log(C_0)$ vs $1000/T$ plot the T_C data measured for both materials in this work and the data measured in the second cycle by Shi et al. [8].

The solid line represents the theoretical curve C_0 vs T_C obtained by Shi et al. [8, Eq. (20)]:

$$C_0 = A \exp\left(-\frac{Q^f}{RT} - \sigma_y \overline{V}_H \frac{2(1+v)}{3(1-2v)RT}\right), \qquad (3)$$

where C_0 is the hydrogen concentration of the material, $\sigma_y = (958 - 1.02T(\mathrm{K}))$ MPa is the yield stress in MPa (applicable from room temperature to 573 K), v and $\overline{V}_H$ are defined in Table 7. $C^f = A \exp\left(-\frac{Q^f}{RT}\right)$ is the hydrogen concentration for hydride precipitation.

From the yield stress data reported in Table 1, two linear regressions were obtained for CANDU and RBMK materials employed in this work: $\sigma_y^{CANDU} = (1103.6 - 1.026\ T(\mathrm{K}))$ MPa and $\sigma_y^{RBMK} = (850.8 - 0.659\ T(\mathrm{K}))$ MPa, respectively, for temperatures between 298 and 573 K.

When σ_y^{CANDU} is introduced in Eq. (3), good correlation is obtained between the experimental T_C data of CANDU and Shi's prediction (C_0 CANDU curve in Fig. 6). Considering that the memory effect is not present at the crack tip C^f was equaled to TSSP1 (Eq. (1)).

For RBMK, instead, the replacement of σ_y^{RBMK} in Eq. (3) predicts higher C_0 values than measured ones. It is necessary to remark that Eq. (1) was measured for CANDU material and, not necessarily, corresponds to the RBMK terminal solid solubility. Solubility during precipitation depends on the accommodation energy generated by the formation of hydride precipitates [3]. Considering the elastic–plastic model, the elastic and plastic components

Table 6
Experimental T_C values of RBMK material and T_P calculated from TSSP2

Specimen	C_0 (ppm)	$T_P(C_0)$ (°C)	T_C (°C)
R-1-1	30 ± 2	211.0	239
R-1-2			241
R-1-3			241
R-2-2	47 ± 2	244.3	271
R-2-1			269
R-2-3			277
R-2-5			271
R-3-1			283
R-3-2	56 ± 3	258.5	285

C_0 is shown only for samples whose hydrogen concentration was effectively measured. Samples with the same second ID number were cut from the same section and should have the same H concentration.

Table 5
Experimental T_C values of CANDU material

Specimen	C_0 (ppm)	$T_P(C_0)$ (°C)	T_C (°C)	$T(\max V_P)$ (°C)	$T(E(L) = C_0)$ (°C)
C-1-1*	24 ± 1	193–198	200	190–198	201–207
C-1-3*			196		
C-2-1	34 ± 2	216–224	245	227–233	224–233
C-3-3	53 ± 3	249–259	273	258–265	258–268
C-3-2			273		
C-3-1			275		
C-3-4			273		
C-3-5			275		
C-4-2*	60 ± 3	260–269	283	269–276	269–278
C-4-3*			293		

The heat treatment for specimens marked with an asterisk (*) was not quite uniform. T_P is calculated from TSSP2 and $T(E(L) = C_0)$ from $E(L)$. $T(\max V_P)$ is estimated from experimental data shown in Fig. 8. C_0 is shown only for samples whose hydrogen concentration was effectively measured. Samples with the same second ID number were cut from the same section and should have the same H concentration.

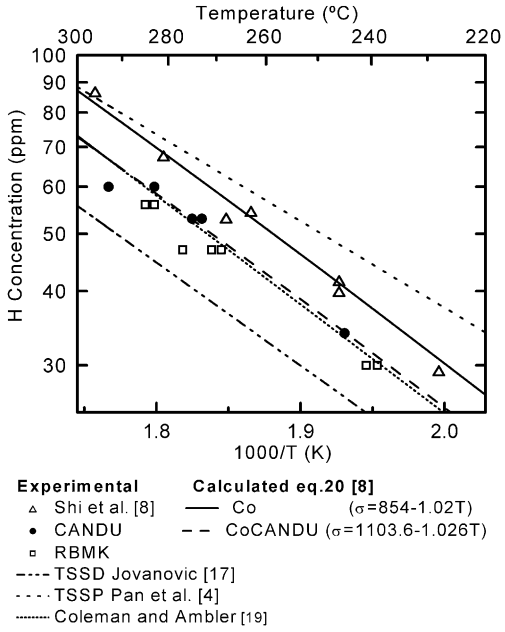

Fig. 6. Experimental values of T_C obtained in CANDU and RBMK tubes for different concentrations. C_0 and C_0 CANDU lines correspond to theoretical curve (Eq. (3)) from Shi et al. [8] with $\sigma_y = 958 - 1.02T$ and $\sigma_y = 1103.6 - 1.026T$, respectively.

of the accommodation energy, generated by the formation of an inclusion, are proportional to σ_y^2 [23]. Consequently, the lower yield stress of the Russian material should provide lower TSSP and subsequent decrease in C_0 (or increase in T_C). A reduction of 10% in TSSP1 is enough to obtain a good adjustment of the RBMK experimental T_C values by Eq. (3).

Using a thermal cycle similar to procedure B employed by Shi et al. [8] to measure T_C, Coleman and Ambler [19] determined the maximum temperature at which crack would grow when cooling to T_T. The corresponding fitting curve is practically overlapped with the C_0 CANDU curve, as shown in Fig. 6.

3.3. Crack propagation rate V_P

Fig. 7 shows the fracture surface of a CCT specimen, where A is the zone pre-cracked by fatigue; B corresponds to different DHC cycles (typical striations can be seen) and C is the final crack by fatigue at room temperature.

The obtained values of V_P are shown in Figs. 8 and 9 for CANDU and RBMK PT's, respectively. The crack propagation in the RBMK material is 60–80% slower than that measured in CANDU PT at the same temperature. Both materials present similar dependence with test temperature:

- For each hydrogen concentration, V_P rises as temperature decreases, from a minimum at T_C to a maximum at a temperature named, from now on, $T(\max V_P)$.
- When $T < T(\max V_P)$, V_P decreases as temperature decreases. Moreover, V_P data measured by using specimens with different hydrogen concen-

Table 7
Parameters used in Puls's model [6]

Parameter	Numerical value	Description
ν	$0.436–4.8\times10^{-4}$ [T(K)-300]	Poisson's ratio [6] (applicable from room temperature to 573 K)
Ω_{Zr}	2.3×10^{-29} m^3/atom	Atomic volume of zirconium [20]
t_{hyd}	1–1.5 μm	Thickness of the crack hydride platelet
N_H	6.13×10^{28} atoms/m^3	Atomic density of the hydride [6]
x	1.6	Number of hydrogen atoms in hydride of composition ZrH_x
$p(r) = (\sigma_{11}+\sigma_{22}+\sigma_{33})/3$		Hydrostatic stress at r
$e^T_{22} = e^T_{33} = 0.0458, e^T_{11} = 0.072$ at l[a]		Hydride (stress free) transformations strains [20]
$e^T_{11} = e^T_{33} = 0.0458, e^T_{22} = 0.072$ at L		
$\overline{V}_H$	16.7×10^{-7} m^3/mol	Molal volume of hydrogen [21]
$\overline{V}_{hyd}$	16.3×10^{-6} m^3/mol hydride	Hydride volume per mole H [20]
$D = D_0\exp(-Q_D/(RT))$	CANDU	Diffusion coefficient [22]
	$D_0 = 2.4\times10^{-3}$ cm^2/s	
	$Q_D = 34\,700$ J/mol	
	RBMK	
	$D_0 = 5.2\times10^{-3}$ cm^2/s	
	$Q_D = 42\,440$ J/mol	

[a] At the crap tip, the normal-to-hydride platelet is parallel to circumferential direction of PT and applied stress, while at L the normal-to-hydride platelet is parallel to radial direction of PT.

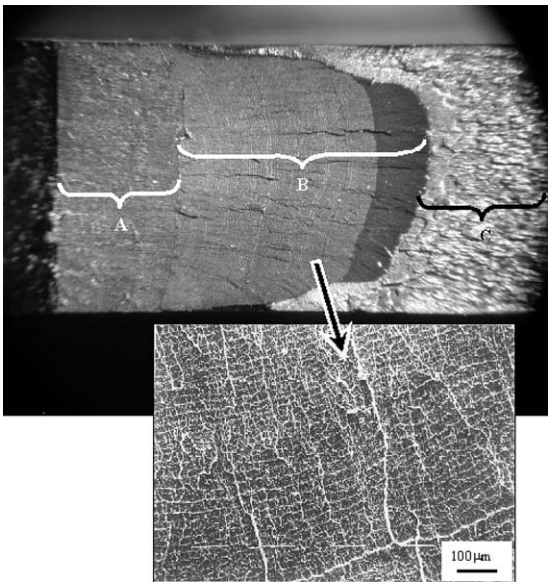

Fig. 7. Typical fracture surface of a CANDU CCT specimen.

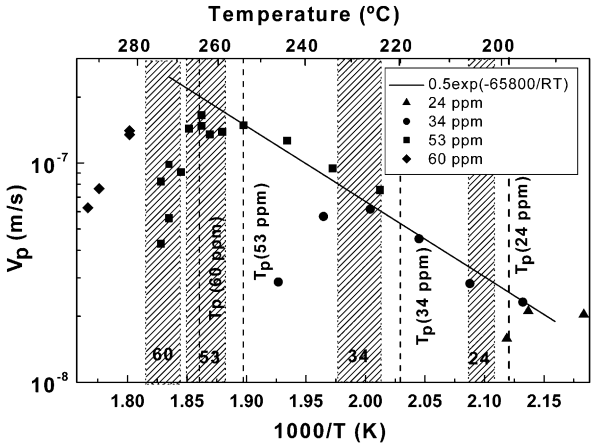

Fig. 8. Crack velocities V_P measured for different temperatures and hydrogen concentrations, in CANDU PT's. The solid line represents the Arrhenius equation: $V_P = A\exp(-Q/RT)$. Ranges of $T(E(L) = C_0)$ marked as shadowed bands.

trations can be represented by an Arrhenius equation: $V_P = A\exp(-Q/RT)$, which is nearly independent of the hydrogen concentration.

Table 8 reports the values of A and Q calculated for each material and those obtained by other authors. Whereas the parameter Q is similar in RBMK and CANDU materials (66–68 kJ/mol), CANDU PT presents a parameter A higher than RBMK and consequently its value of V_P is higher.

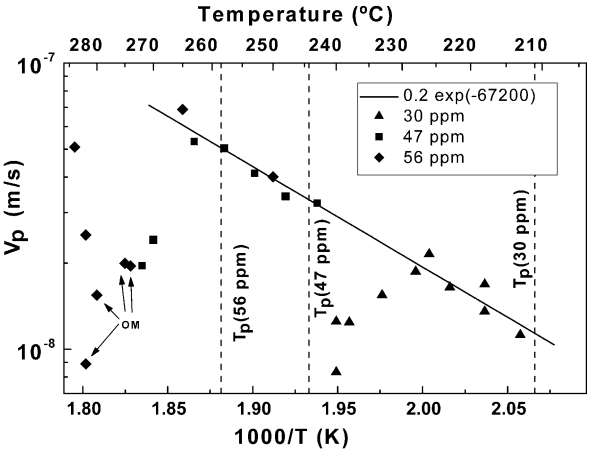

Fig. 9. Crack velocities V_P measured for different temperatures and hydrogen concentrations, in RBMK PT's. The solid line represents the Arrhenius equation: $V_P = A\exp(-Q/RT)$. OM points out tests made with Overcharging Method, which affected the results obtained in this material.

Table 8
Parameters of Arrhenius law $V_P = A\exp(-Q/RT)$

PT	A (m/s)	Q (kJ/mol)
CANDU	0.5	65.8
RBMK	0.2	67.2
Other authors:		
Simpson–Puls [5]	0.27	65.5
Kim [24]	0.0032	38–42
Ambler [9]	0.68	71.5
Sagat [25]	0.053	60.0

From the work of Puls [6] crack propagation velocity, with precipitated hydride in the bulk, may be expressed as

$$V_P = 2\pi D(E(L) - E(l))/(\Omega_{Zr} \cdot \Phi(L,l) \cdot t_{hyd} \cdot N_H \cdot x), \quad (4)$$

where

- l is the distance from the crack tip to the center of plastic zone and L is the distance from crack tip to source hydrides.
- $E(L,l)$ is the terminal solid solubility of hydrogen in presence of applied stresses, that can be expressed as

$$E(L,l) = C^S(L,l)\exp[(\overline{W}_t^a(L,l) + p(L,l)\overline{V}_H)/RT]. \quad (5)$$

- $C^S = A\exp(-Q/RT)$ is the solubility without external applied stresses.

- $\overline{W}_{\mathrm{t}}^{\mathrm{a}}(L,l) = -\overline{V}_{\mathrm{hyd}} \sum \sigma_{i,j} e_{i,j}$ is the total interaction energy per mole of hydrogen due to hydride formation under external stress.
- $p(L,l)\overline{V}_{\mathrm{H}}$ is the interaction energy of hydrogen in solution, this term drops out under a stress gradient [6], so it is zero at l.
- $\Phi(L,l) = \int_l^L \exp(p(r)\overline{V}_{\mathrm{H}}/RT) \cdot \mathrm{d}r/r$.
- $D = D_0 \exp(-Q_{\mathrm{D}}/(RT))$ is the diffusion coefficient.
- Other parameters are described in Table 7.

At L, for plain strain conditions, $\sigma_{11} = \sigma_{22} = K_{\mathrm{I}}/\sqrt{2\pi L}$ and $\sigma_{33} = 2\nu K_{\mathrm{I}}/\sqrt{2\pi L}$; in this work $K_{\mathrm{I}} = 15\ \mathrm{MPa\ m^{1/2}}$.

As K_{I} was high enough, it is feasible to assume that the hydride grew and fractured inside the plastic zone. The tensile stress in the plastic zone may be calculated using the Hutchinson, Rice and Rosengren singular solution, then at l: $\sigma_{11} = 3.35\sigma_{\mathrm{y}}$, $\sigma_{22} = 2.08\sigma_{\mathrm{y}}$ and $\sigma_{33} = 2.71\sigma_{\mathrm{y}}$, where σ_{y} is the yield stress [6].

In the present work V_{P} has been calculated by employing Eqs. (4) and (5), taking into account the next considerations:

- Assuming that the hydride at the crack tip is fully fractured, a new platelet must be nucleated in each thermal cycle, then $C^{\mathrm{S}}(l)$ may be replaced by TSSP1 (Eq. (1)).
- When the test temperature is lower than $T(\max V_{\mathrm{P}})$, $C^{\mathrm{S}}(L)$ must be equal to TSSP2 (Eq. (2)), because the hydrogen concentration in the bulk is in equilibrium with hydride particles which have precipitated during cooling from a T_{S} temperature lower than 330 °C.
- Distance l was taken as the length of the striations observed on the fracture surface, nearly 20 μm (see Fig. 7).
- Distance L was chosen as the mean separation between hydride particles, nearly 50–100 μm along axial direction on the R–A plane of PT.
- According to observations made in previous work, the thickness t_{hyd} of hydride platelets may range between 1 and 1.5 μm. The diffusion coefficients were taken from Skinner and Dutton [22], these authors investigated the effect of different previous heat treatments on the diffusivity of H in Zr–2.5Nb PT's. We use the coefficient measured in autoclaved condition for the CANDU PT and the autoclaved plus a heat treatment at 565 °C, 24 h for the RBMK PT, because these conditions are similar to the fabrication routes of Canadian and Russian tubes, respectively.

Both coefficients were measured in the axial direction and are reported in Table 7.

The experimental data obtained for both PT's when $T_{\mathrm{T}} < T(\max V_{\mathrm{P}})$ and the calculated curves of

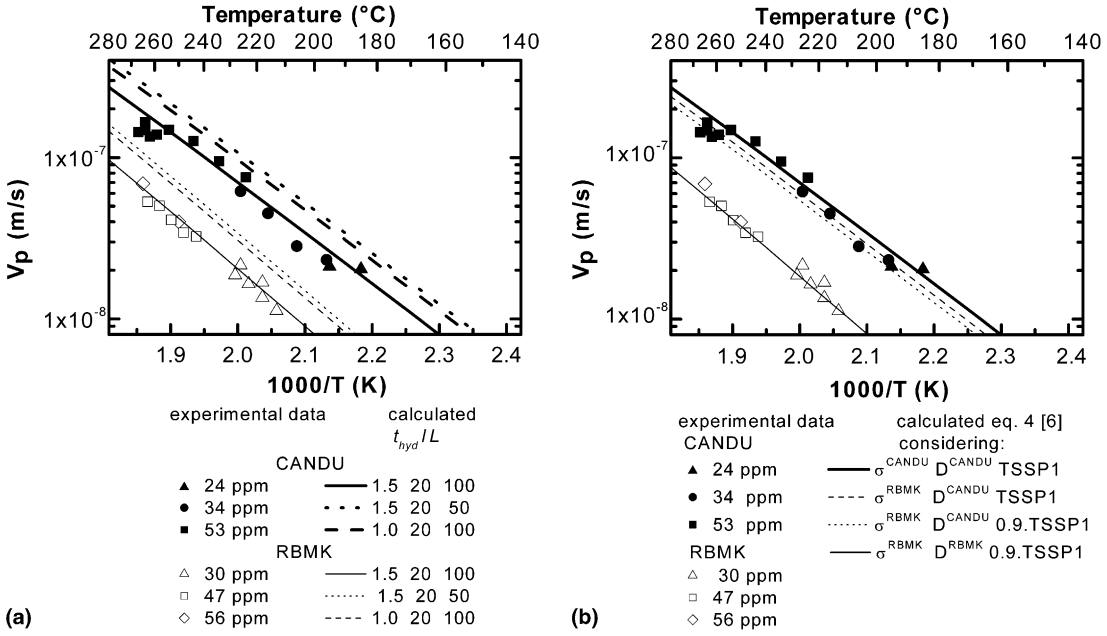

Fig. 10. Crack velocities V_{P} measured in CANDU and RBMK PT's for $T < T(\max V_{\mathrm{P}})$ and calculated according to Eq. (4) [6]: (a) with different parameters t_{hyd} and L; (b) with different values of diffusion coefficient D, TSSP and σ_{y}.

V_P, assuming L and t_{hyd} values in the measured range, are plotted in Fig. 10(a). The best correlation was obtained when $t_{hyd} = 1.5$ μm and $L = 100$ μm. The spread introduced by the uncertainty on t_{hyd} and L is not enough to justify the gap between the RBMK and CANDU data, as shown in the graphic.

It is important to remark that if only the reduction in yield stress of the RBMK is considered in Eqs. (4) and (5) (and if D and TSSP remain the CANDU values), V_P decreases 15–20% approximately (Fig. 10(b) – dashed line). If, besides, a reduction of 10% (as discussed in Section 3.2) is applied to TSSP1 and TSSP2 V_P decreases 25–30% (Fig. 10(b) – dotted line). The main decrease in the calculated V_P is provided by the reduction of the diffusion coefficient that results in a final RBMK V_P value (Fig. 10(b) – fine solid line) which is (65–80%) lower than that of CANDU (Fig. 10(b) – thick solid line). In CANDU material the ligaments of the β phase surrounding the elongated α grains provide fast-diffusion paths for hydrogen along axial direction [22]. The higher ageing temperature at which RBMK is exposed during its fabrication route produces spheroidization and a more homogeneous β-phase distribution and, likely, break up of β-Zr into β-Nb and α phases (this later point must be corroborated). These effects would be responsible of the slower diffusion along axial direction and consequently, added to the lower yield stress, would produce slower V_P.

In the range of the studied temperatures, the values obtained according to Puls's theory may be adjusted by an Arrhenius equation with an activation energy $Q = 59.6$ kJ/mol. This value is close to that calculated from the experimental data (66 kJ/mol).

As can be observed in Figs. 8 and 9 the maximum value of V_P, measured for each hydrogen concentration, is obtained for a temperature higher than T_P. In Table 5, the sixth column reports an estimated range for this temperature named as $T(\max V_P)$. This unexpected result may be explained if we consider that the external applied stress affects the solubility not only at the crack tip ($l = 20$ μm) but in the neighborhood too ($L = 100$ μm). Although the effect on $E(L)$ is much lower than on $E(l)$, (0.43–0.48) kJ against (5.0–3.9) kJ, as can be seen in Table 9, it can displace the precipitation approximately 10–15 °C to higher values. At this temperature $E(L)$ will reach its maximum possible value ($E(L) = C_0$) and so will do V_P. The seventh column in Table 5 shows the precipitation temperatures

Table 9
Interaction energy (kJ) due to the presence of an external stress, calculated in the temperature range 150–300 °C, near the crack tip (l) and in the neighborhood (L)

	T (°C)	$\overline{W}_t^a(L,l)$ (kJ)	$p\overline{V}_H$ (kJ)	$\overline{W}_t^a(L,l) + p\overline{V}_H$ (kJ)
L	150	−1.4	0.92	−0.48
	300	−1.3	0.87	−0.43
l	150	−5.0	0	−5.0
	300	−3.9	0	−3.9

$T(E(L) = C_0)$ calculated from $E(L)$ for each measured concentration with their error. The same is shown as shadowed bands plotted in Fig. 8. For each concentration, $T(\max V_P)$ values are located inside these bands (worst correlation is observed for specimens C-1 and C-4 for which the first heat treatment was not quite uniform).

Although Eq. (4) was developed under the assumption that hydride particles are present in the bulk [5], a similar dependence of V_P with the difference $(E(L) - E(l))$ may be accepted at temperatures higher than $T(\max V_P)$. Assuming that hydrogen is fully in solution, $E(L)$ equals the hydrogen concentration of the specimens C_0. Fig. 11 shows the values of V_P calculated for the specimens CANDU with 34 and 53 ppm using these assumptions. Even though no good agreement is achieved, the qualitative behavior is well reproduced.

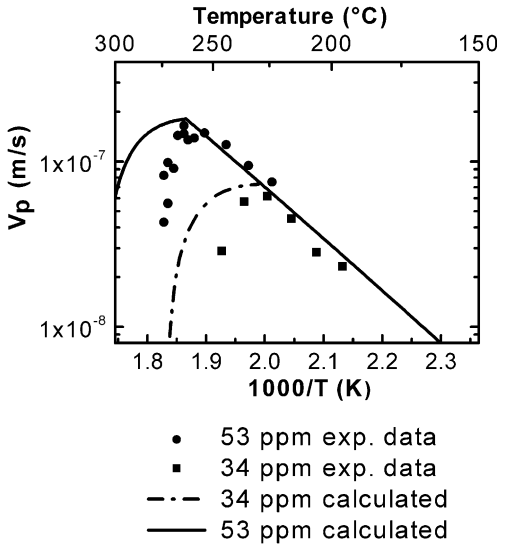

Fig. 11. Crack velocities V_P measured in CANDU material with 34 and 53 ppm and V_P calculated with Eq. (4) [6] assuming that in the range $T_C > T > T(\max V_P)$: $C^S(L) = C_0$ and for $T < T(\max V_P)$: $C^S(L) =$ TSSP2.

4. Conclusions

DHC tests carried out on specimens cut from two pressure tubes (CANDU and RBMK) charged with different hydrogen concentrations and tested at various temperatures, cooling the specimens from solution, have shown

1. the highest temperature at which DHC starts (T_C) is neither affected by memory effect of hydrides precipitated at the crack tip nor by the type of initial crack (fatigue or DHC), in the present test conditions;
2. for each hydrogen content C_0, T_C is higher than the bulk precipitation temperature (T_P). The experimental values (C_0, T_C) measured for CANDU PT agree very well with the theoretical prediction of Shi et al. [8];
3. for each hydrogen concentration, the crack propagation rate V_P presents a maximum at a temperature $T(\max V_P) > T_P$. This temperature may be estimated from the precipitation curve adding the effect of external stresses on solubility at the crack neighborhood: $E(L) = \mathrm{TSSP2}\exp(\overline{W}_t^a(L) + p(L)\overline{V}_H/RT)$;
4. when hydrides are precipitated in the bulk, at $T < T(\max V_P)$, V_P shows an Arrhenius dependence with T, ($V_P = A\exp(-Q/RT)$), irrespective of the hydrogen concentration. The adjusted value of Q is 66–68 kJ for both studied materials;
5. V_P of CANDU PT is 65–80% higher than that one of RBMK PT. This result may be mainly attributed to the higher diffusivity of hydrogen in the aligned β phase of CANDU material and, in a lesser extent, to its higher yield stress.

Acknowledgements

The authors always remain grateful to the memory of Mr. P. Coronel for his aid in sample preparation and gratefully acknowledge the technical assistance of A. Loberse and C. Lafont. The authors wish to thank Dr C. Coleman for his valuable discussion. Both CANDU and RBMK material have been supplied by the International Atomic Energy Agency, in the frame of the Cooperative Research Program on 'Hydrogen and hydride induced degradation of the mechanical and physical properties of zirconium-based alloys', 1999–2002.

References

[1] D.O. Northwood, U. Kosasih, Int. Metals Rev. 28 (2) (1983) 92.
[2] R. Dutton, K. Nuttall, M.P. Puls, L.A. Simpson, Met. Trans. A 8 (1977) 1153.
[3] G.F. Slattery, J. Inst. Metals 95 (1967) 2391.
[4] Z.I. Pan, I.G. Ritchie, M.P. Puls, J. Nucl. Mater. 228 (1996) 227.
[5] L.A. Simpson, M.P. Puls, Met. Trans. A 10 (1979) 1093.
[6] M.P. Puls, Met. Trans. A 21 (1990) 2905.
[7] S.Q. Shi, M. Liao, M.P. Puls, Model. Simul. Mater. Sci. Eng. 2 (1994) 1065.
[8] S.Q. Shi, G.K. Shek, M.P. Puls, J. Nucl. Mater. 218 (1995) 189.
[9] J.F.R. Ambler, in: D.G. Franklin, R.B. Adamson (Eds.), Zirconium in the Nuclear Industry, 6th International Symposium, ASTM STP 824, Philadelphia, 1984, p. 653.
[10] Delayed hydride cracking in zirconium alloys in pressure tube nuclear reactors, IAEA TECDOC 1410, Final report of a coordinated research project, 1998–2002, October 2004.
[11] J.J. Kearns, J. Nucl. Mater. 22 (1967) 292.
[12] A.D. Lepage, W.A. Ferris, G.A. Ledoux, Procedure for adding hydrogen to small sections of zirconium alloys, FC-IAEA-03, T1.20.13-CAN-27363-03, November 1998.
[13] J.J. Kearns, J. Nucl. Mater. 43 (1972) 336.
[14] Standard test method for plane-strain fracture toughness of metallic materials, ASTM E-399-83, 1983.
[15] Standard test method for measurement of fatigue crack growth rates, ASTM E647-95a, 1995, p. 577.
[16] Standard test method for J_{IC}, a measure of fracture toughness, ASTM E813-81.
[17] M. Jovanovic, A. Stern, H. Kneis, G.C. Weatherly, M. Leger, Can. Metall. Quarterly 27 (4) (1988) 323.
[18] A. Sawatzky, J.S. Wilkins, J. Nucl. Mater. 22 (1967) 304.
[19] C.E. Coleman, J.-F.R. Ambler, Scripta Met. 17 (1983) 77.
[20] G.J.C. Carpenter, J. Nucl. Mater. 48 (1960) 264.
[21] S.R. MacEwen, C.E. Coleman, C.E. Ells, J. Faber Jr., Acta Metall. 33 (1985) 753.
[22] B.C. Skinner, R. Dutton, in: N.R. Moody, A. Thompson (Eds.), Hydrogen Effects on Material Behavior, The Minerals, Metals and Materials Society, Pennsylvania, 1990, p. 73.
[23] B.W. Leicth, M.P. Puls, Met. Trans. A 23 (1992) 2905.
[24] S.S. Kim, S.Ch. Kwon, Y.S. Kim, J. Nucl. Mater. 273 (1999) 52.
[25] S. Sagat, C. Coleman, M. Griffiths, B. Wilkins, in: A.M. Garde, E.R. Bradley (Eds.), Zirconium in the Nuclear Industry: 10th International Symposium, ASTM STP 1245, ASTM, Philadelphia, 1994, p. 35.